Electronic Supplementary Material (ESI) for Journal of Materials Chemistry C.

Supporting information

Design of highly efficient energy transfer phosphor $Sr_4Al_{14}O_{25}$: Eu^{2+}, Mn^{4+} in deep-red emitting with application potential in plant growth

Cancan Li [1], Yunpeng Zhou [1], Takatoshi Seto [1,], Yuhua Wang [1,*]*

[1] Key Laboratory for Special Function Materials and Structural Design of the Ministry of Education,

National & Local Joint Engineering Laboratory for Optical Conversion Materials and Technology of National Development and Reform Commission, Department of Materials Science,

School of Materials and Energy, Lanzhou University, No. 222, South Tianshui Road, Lanzhou, Gansu, 730000, P. R. China,

*Corresponding author: Takatoshi Seto - E-mail: seto@lzu.edu.cn

Yuhua Wang - E-mail: wyh@lzu.edu.cn

ID 0000-0002-3928-2557 (T. Seto), ID 0000-0001-7047-4760 (Y. Wang)

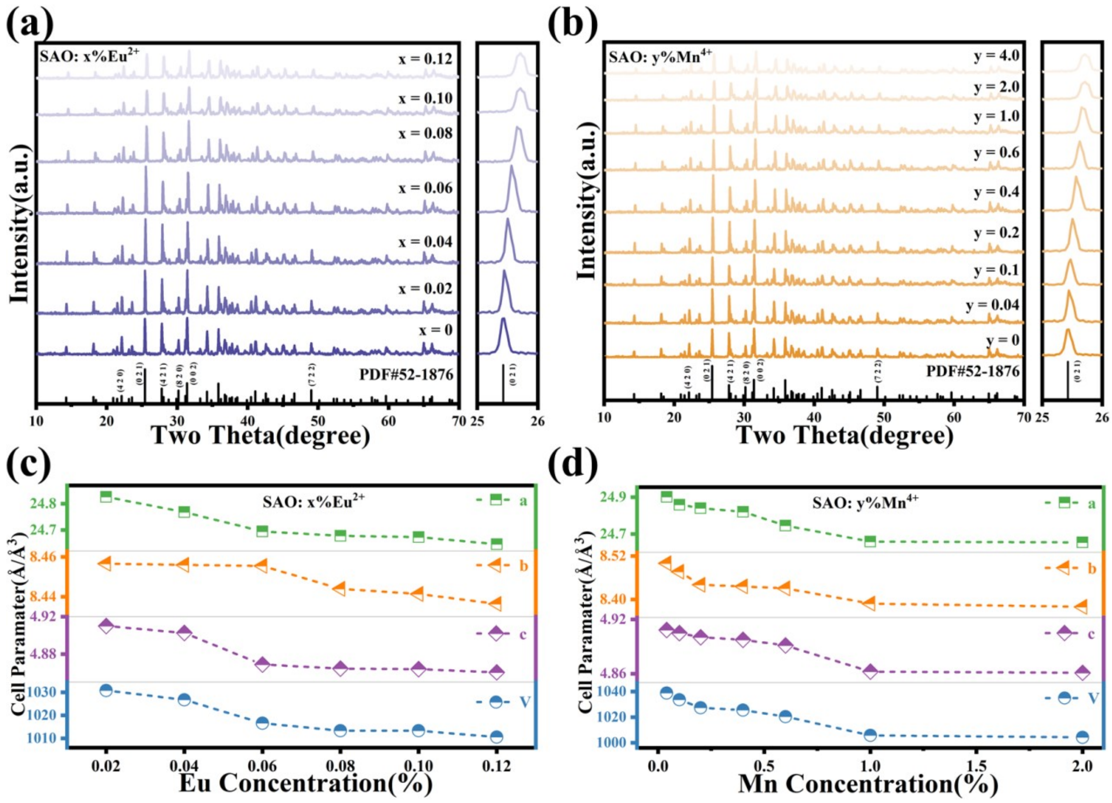

Fig. S1 (a) and **(b)** are XRD patterns of SAO: x%Eu^{2+} and SAO: y%Mn^{4+}. Rights are the peak shifts of (0 2 1). (0≤x%≤0.12%, 0≤y%≤4.0%) **(c)** Dependence of lattice parameters and unit cell volume on Eu^{2+} concentration and **(d)** Mn^{4+} concentration.

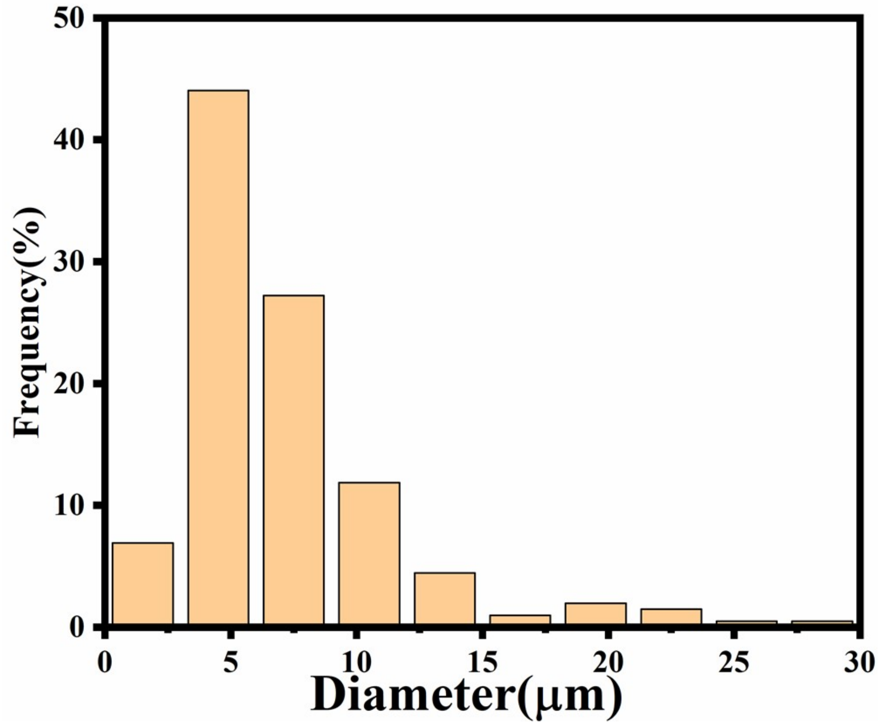

Fig. S2 SEM particle size distribution of SAO: Eu^{2+}, Mn^{4+}.

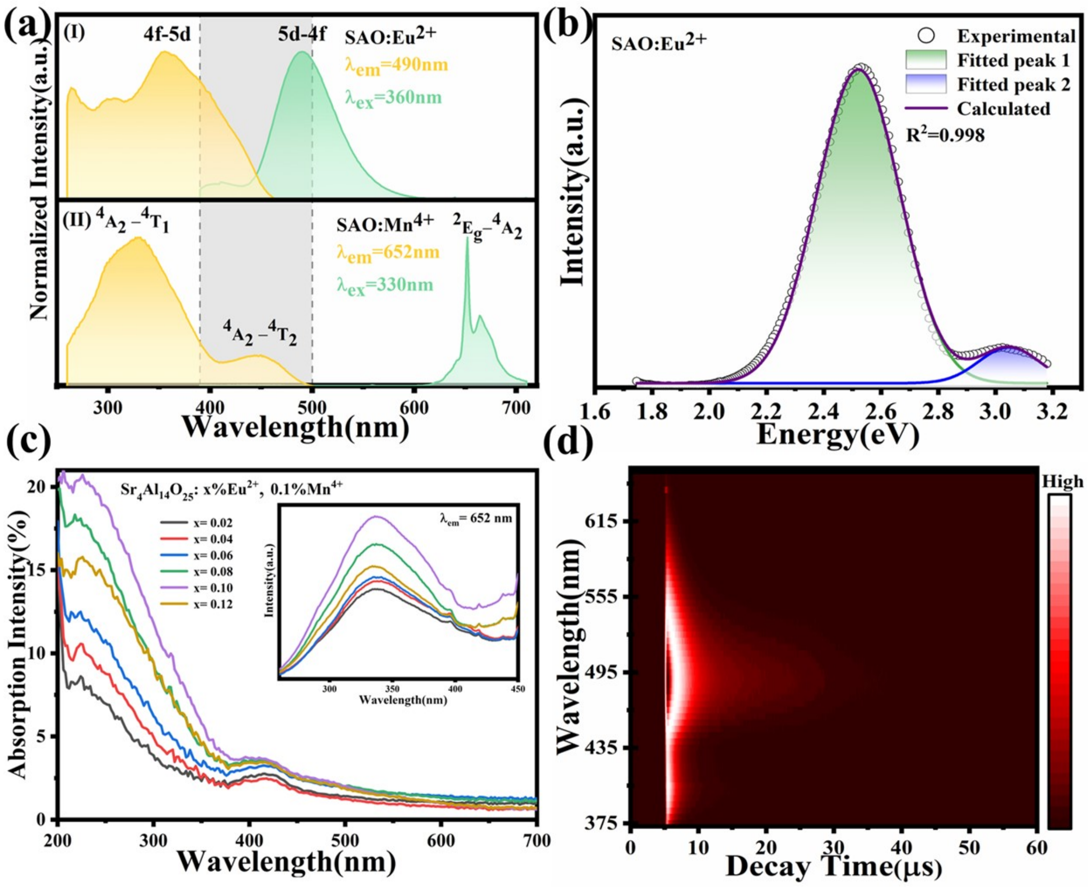

Fig. S3(a) PLE and PL spectra of SAO: Eu^{2+}; SAO: Mn^{4+}. **(b)** Gauss fitting of PL in SAO: 0.1%Eu^{2+}. **(c)** The absorption spectra of SAO: x%Eu^{2+}, 0.1%Mn^{4+}, (0.02≤ x%≤0.12%). Inset shows relative PLE spectra monitored at 652 nm. **(d)** TRPL of SAO: 0.1%Eu^{2+}.

Note：Fig. S3(a) (I) performs the excitation and emission peak of SAO: 0.1%Eu^{2+}. The excitation of Eu^{2+} has a large broad band range from 240 nm to 480 nm peaked at 360 nm. The emission spectrum exhibits a large broad band from 380 nm to 600 nm with peak located at 490 nm. As shown in **Fig. S3(b)**, the emission can be well-fitted into two Gaussian peaks appeared at 407 nm (3.047 eV) and 492 nm (2.521 eV). **Fig. S3(d)** presents the time-resolved photoluminescence (TRPL) mapping of Eu^{2+}, which has the same shape as the PL spectrum shown in **Fig. S3(a) (I)**. And it clearly reveals the two peaks of Eu^{2+} and can also directly prove the two luminescent centers of Eu^{2+}. As displayed in **Fig. 1(d)**, Eu^{2+} can occupy two types of Sr^{2+} due to the similar radius of two ions, causing two types of emission centers. Generally, the Van Uitert empirical equation below was involved to collect the energy of emission peak (E): [1-3]

$$E(cm^{-1}) = Q \times [1 - (\frac{V}{4})^{\frac{1}{V}} \times 10^{\frac{-nrE_a}{80}}] \tag{1}$$

where Q and V represent the lower d-band edge and valence state of Eu^{2+}, respectively. E_a is the anion's electron affinity. r and n refer to the radius and the coordination number of the cation substituted, respectively. In this system, the E_a and V are constant, so E is determined by the values of r and n. The higher the value of nr, the higher the value of E, and the shorter the emission wavelength. Hence, the emission peak at 407 nm is ascribed to the Eu^{2+} occupying the Sr_2 sites with ten-coordination, while the longer wavelength peaked at 492 nm can be attributed to Eu^{2+} occupying the Sr_1 site with seven-coordination.

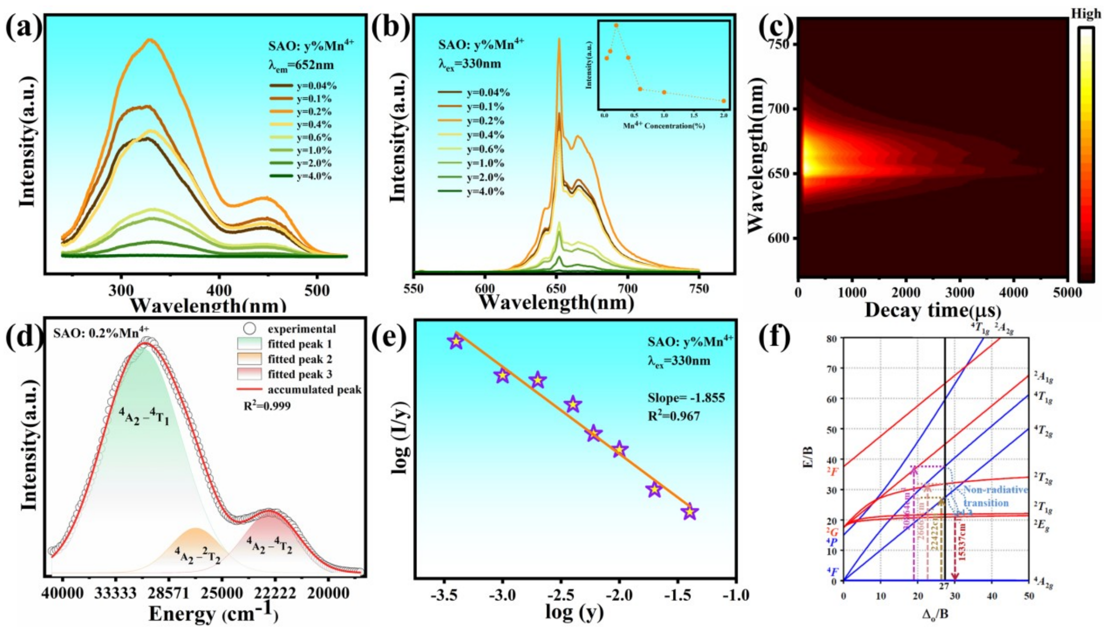

Fig. S4(a) PLE spectra of SAO: y%Mn^{4+} (0.04%≤ y%≤4.0%). **(b)** PL spectra of SAO: y%Mn^{4+}. Inset shows emission intensity on different Mn^{4+} concentrations. **(c)** TRPL spectrum of SAO: 0.2%Mn^{4+}. **(d)** Gauss fitting of PLE spectrum of SAO: 0.2%Mn^{4+}. **(e)** The functional dependence of log (I/y) on log (y). **(f)** Tanabe-Sugano energy level diagram of SAO: 0.2%Mn^{4+}.

Note: In this work, the main part is about Mn^{4+}. **Fig. S4(a)** and **(b)** illustrate the excitation (λ_{em}=652 nm) and emission (λ_{ex}=330 nm) spectra of series samples SAO: y%Mn^{4+} (0 ≤ y% ≤ 4.0%). The PLE spectra have a broad range from 270 nm to 550 nm. As for the PL spectra of Mn^{4+}, under the excitation spectra of Mn^{4+} at 330 nm, the emission spectra present a red-emitting narrow band from 600 nm to 750 nm with peak at 652 nm and with a full width at half maximum (FWHM) of 23-27 nm, which matches well with the absorption range of chlorophyll A, and chlorophyll B in plants. The inset in **Fig. S4(b)** describes the relationship between emission intensity on Mn^{4+} concentration, where both the excitation intensity and the emission intensity first increase with the increasing of the Mn^{4+} ion doping concentration, and when y% reaches 0.2%, both reach the maximum value, and then their intensities gradually decrease as the continuous rising of the Mn^{4+} ion. In order to clarify the situation related to the luminescent center in the SAO: 0.2%Mn^{4+}, a series of decay curves of the samples were monitored under the excitation of Mn^{4+} at 330 nm from 570 nm to 770 nm in 4 nm steps. **Fig. S4(c)** depicts the time-resolved photoluminescence (TRPL) mapping. It appears to have a similar shape with the PL spectrum, without the shifting of the PL peak at 652nm over the entire range from 10 to 6000μs, indicating that only one type of luminescent center exists in SAO: 0.2%Mn^{4+}.

To further study the concentration quenching behavior of SAO: y%Mn^{4+} samples, it's wise to take the critical distance R_c into consideration, and its value can be calculated by the following formula: [4]

$$R_c \approx 2\left[\frac{3V}{4\pi x_c Z}\right]^{1/3} \tag{2}$$

In which, V represents the unit cell volume, x_c represents the critical doping concentration of Mn^{4+} ions, and Z represents the number of units in the unit cell. For SAO: 0.2%Mn^{4+} phosphor, V=1016.75Å^3, x_c =0.002 and Z=2, so the calculated Rc is 7.86 nm. This value is much larger than the interaction distance of 5 Å between the activator ions, thus the concentration quenching behavior of SAO: y%Mn^{4+} belongs to the multipolar-multipolar interaction, which can be divided into dipole-dipole(d-d), dipole-quadrupole(d-q), quadrupole-quadrupole(q-q), three types. These three types can be distinguished in accordance with the value of θ, which are able to be calculated according to Dexter's theory by the following formula: [5]

$$\frac{I}{y} = k[1 + \beta(y)^{\theta/3}]^{-1} \tag{3}$$

Where the symbol *I* represents the emission intensity, y represents the Mn^{4+} doping concentration, and k and β(y) are related to the excitation conditions and the specific lattice matrix, respectively. θ values are 6, 8, 10, corresponding to d-d, d-q, q-q interactions, respectively.

The value of θ is usually given by the slope of the functional dependence of log(I/y) on log(y). As can be seen from **Fig. S4(e)**, under the excitation of 330 nm, the slope of the fitting curve is -1.855. The calculated θ values 5.565, closing to 6, which indicates that the SAO: y%Mn^{4+} concentration quenching mechanism belongs to d-d interaction type.

As exhibited in **Fig. S4(d)**, the excitation spectra can be well fitted into three Gaussian peaks located at 30864 cm^{-1}(324 nm), 26667 cm^{-1}(375 nm), 22422 cm^{-1}(446 nm), and ascribed to $^4A_2 \rightarrow {}^4T_1$, $^4A_2 \rightarrow {}^2T_2$, and $^4A_2 \rightarrow {}^4T_2$ transition of Mn^{4+}, respectively. It is noticed that the two peaks at 375 nm and 446 nm are able to be matched well with the emission spectra of Eu^{2+} shown in **Fig. S3(a)**, suggesting that it satisfies the condition of energy transfer.

The splitting of energy levels for Mn^{4+} affected by the crystal field environment can usually be expressly illustrated through the Tanabe-Sugano (TS) diagram in **Fig. S4(f)**. In general, the crystal field can be determined by three parameters, namely the crystal field intensity Dq, Racah parameters B and C. They are directly related to the PLE and PL spectra, and these values can be estimated from following functions: [6]

$$Dq = \frac{E(^4A_2 - {}^4T_2)}{10} \tag{4}$$

$$\frac{D_q}{B} = \frac{15(x-8)}{(x^2 - 10x)} \tag{5}$$

$$x = \frac{E(^4A_2 - {}^4T_1) - E(^4A_2 - {}^4T_2)}{D_q} \tag{6}$$

$$\frac{E(^2E_g - ^4A_2)}{B} = \frac{3.05C}{B} + 7.9 - \frac{1.8B}{D_q} \qquad (7)$$

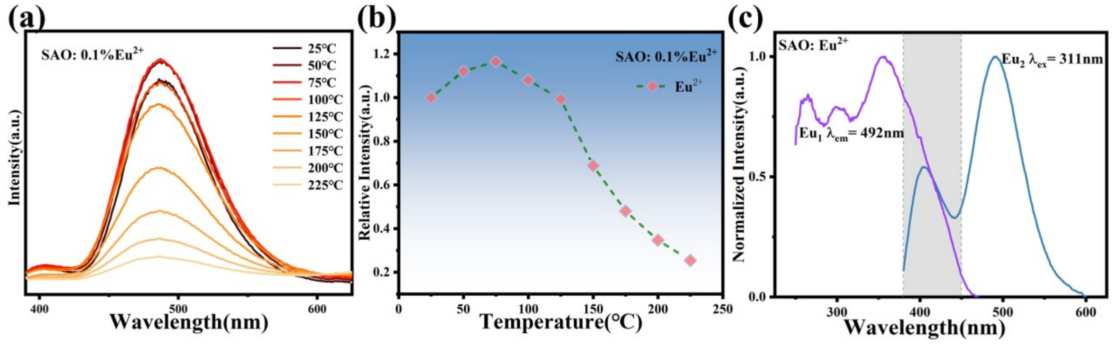

Fig. S5(a) PL spectra and **(b)** relative emission intensity of SAO: Eu^{2+} at different temperatures. (c) The normalized emission spectrum of Eu_2 (monitored at 311 nm) and excitation spectrum of Eu_1 (monitored at 492 nm). (The grey area means the overlapped region).

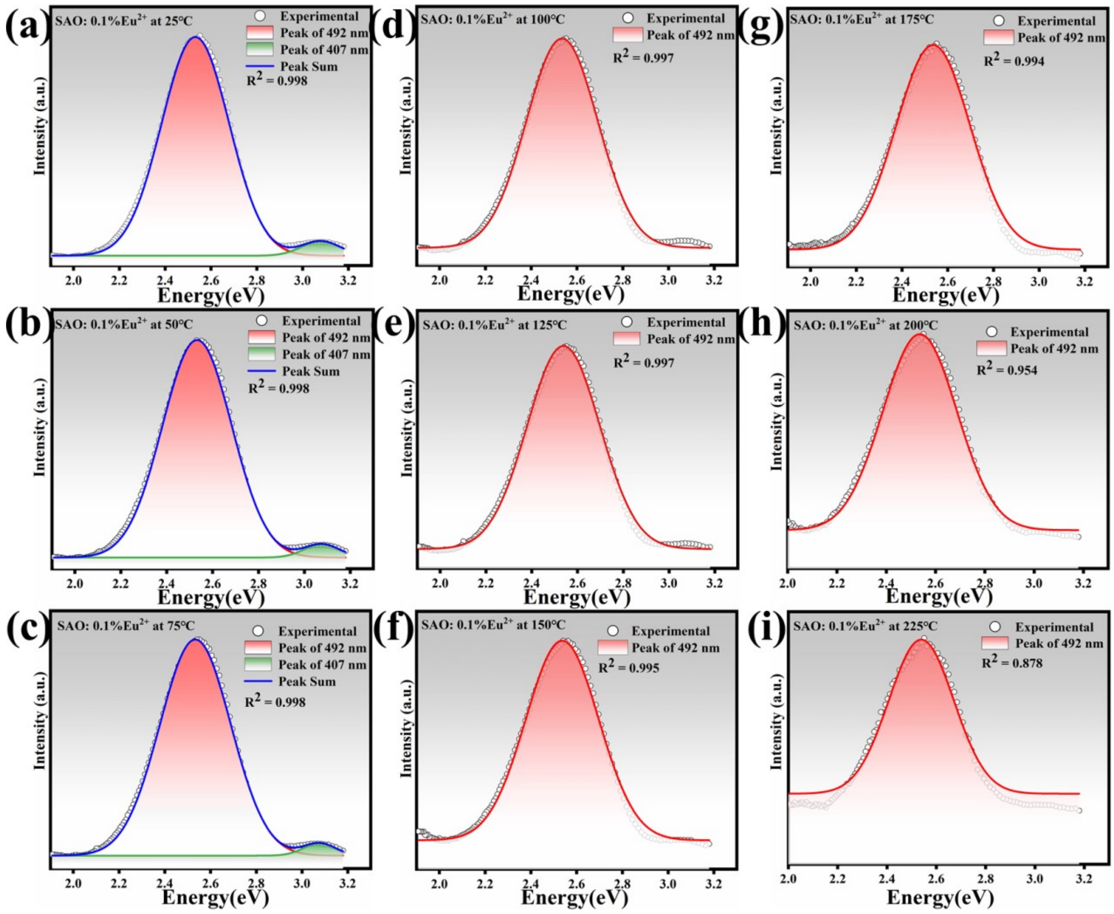

Fig. S6 The fitting peaks in PL spectra of SAO: Eu at different temperatures. (a)25°C, (b)50°C, (c)75°C, (d)100°C, (e)125°C, (f)150°C, (g)175°C, (h)200°C, (i)225°C.

Table S1 Matrix sample structure refinement information of $Sr_4Al_{14}O_{25}$

Formula	$Sr_4Al_{14}O_{25}$

Crystal System	Orthorhombic
Space-group	*P* m m a
a (Å)	24.69(7)
b(Å)	8.45(4)
c(Å)	4.87(0)
α=β=γ(°)	90°
V(Å^3)	1016.755
R_{wp}	0.1133
Rp	0.0847
χ^2	1.798

Table S2. Refined atomic coordinates and ionic occupancies of SAO host

Atom	x	y	z	Occupancy
Sr_1	0.1382100(0)	0.5000000(0)	0.0334460(0)	1.000
Sr_2	0.12176300(0)	0.0000000(0)	0.1106860(0)	1. 000
Al_1	0.1818550(0)	0.1890570(0)	0.6399910(0)	1.000
Al_2	0.0633530(0)	0.3154890(0)	0.4889800(0)	1.000
Al_3	0.2500000(0)	0.3055320(0)	0.1498890(0)	1.000
Al_4	0.0000000(0)	0.1817030(0)	0.0000000(0)	1.000
Al_5	0.0000000(0)	0.0000000(0)	0.50000000(0)	1.000
Al_6	0.0000000(0)	0.5000000(0)	0.0000000(0)	1.000
O_1	0.0438010(0)	0.1425280(0)	0.3130020(0)	1.000
O_2	0.1400690(0)	0.3341260(0)	0.4950880(0)	1.000
O_3	0.1957760(0)	0.2345220(0)	-0.0380520(0)	1.000
O_4	0.2500000(0)	0.2516130(0)	0.4472130(0)	1.000
O_5	0.0283410(0)	0.0000000(0)	0.81458160(0)	1.000
O_6	0.0435740(0)	0.5000000(0)	0.3048650(0)	1.000
O_7	0.1662780(0)	0.0000000(0)	0.5867110(0)	1.000
O_8	0.0436640(0)	0.3402850(0)	0.8529530(0)	1.000
O_9	0.2500000(0)	0.5000000(0)	0.1103960(0)	1.000

Table S3. Coordinate and band lengths of Sr_1 in SAO host

Vector	Length/Å
Sr_1-O_1	2.583(17)
Sr_1-O_1	2.583(17)
Sr_1-O_3	2.683(17)
Sr_1-O_3	2.683(17)
Sr_1-O_5	2.47(3)
Sr_1-O_7	2.85(3)
Sr_1-O_7	2.51(3)

Table S4. Coordinate and band lengths of Sr_2 in SAO host

Vector	Length/Å
Sr_2-O_2	2.97859(8)
Sr_2-O_2	2.65449(6)
Sr_2-O_2	2.97859(8)
Sr_2-O_2	2.65449(6)
Sr_2-O_3	2.68350(6)
Sr_2-O_3	2.68350(6)
Sr_2-O_6	2.68910(6)
Sr_2-O_8	2.84108(5)
Sr_2-O_8	2.84108(5)
Sr_2-O_9	2.79015(7)

Table S5. Coordinate and band lengths of Al_1 in SAO host

Vector	Length/Å
Al_1-O_2	1.75398(3)
Al_1-O_3	1.65347(5)
Al_1-O_4	2.00135(4)
Al_1-O_7	1.66685(4)

Table S6. Coordinate and band lengths of Al_2 in SAO host

Vector	Length/Å
Al_2-O_1	1.76507(4)
Al_2-O_2	1.90412(5)
Al_2-O_6	1.86726(4)
Al_2-O_8	1.85307(5)

Table S7. Coordinate and band lengths of Al_3 in SAO host

Vector	Length/Å
Al_3-O_3	1.73214 (3)
Al_3-O_3	1.73214(3)
Al_3-O_4	1.52060(4)
Al_3-O_9	1.65780(4)

Table S8. Coordinate and band lengths of Al_4 in SAO host

Vector	Length/Å
Al_4-O_1	1.90132(4)
Al_4-O_1	1.90132(4)
Al_4-O_5	1.91755(4)
Al_4-O_5	1.91755(4)
Al_4-O_8	1.86645(3)
Al_4-O_8	1.86645(3)

Table S9. Coordinate and band lengths of Al_5 in SAO host

Vector	Length/Å
Al_5-O_1	1.86065(3)
Al_5-O_1	1.86065(3)
Al_5-O_1	1.86065(3)
Al_5-O_1	1.86065(3)
Al_5-O_5	1.68684(4)
Al_5-O_5	1.68684(4)

Table S10. Coordinate and band lengths of Al_6 in SAO host

Vector	Length/Å
Al_6-O_6	1.83664(4)
Al_6-O_6	1.83664(4)
Al_6-O_8	1.87337(3)
Al_6-O_8	1.87337(3)
Al_6-O_8	1.87337(3)
Al_6-O_8	1.87337(3)

Table S11 Distances between Sr_1 and Al atoms in SAO host

Vector	Length/Å
Sr_1-Al_1	3.169186)
Sr_1-Al_1	3.38209(7)
Sr_1-Al_1	3.16918(6)
Sr_1-Al_1	3.38209(7)
Sr_1-Al_2	3.55360(6)
Sr_1-Al_2	3.55360(6)
Sr_1-Al_4	3.42451(7)
Sr_1-Al_4	3.42451(7)
Sr_1-Al_5	3.56030(7)

Table S12 Distances between Sr_2 and Al atoms in SAO host

Vector	Length/Å
Sr_2-Al_1	3.43230(7)
Sr_2-Al_1	3.43230(7)
Sr_2-Al_2	3.59485(7)
Sr_2-Al_2	3.28733(6)
Sr_2-Al_2	3.59485(7)
Sr_2-Al_2	3.28733(6)
Sr_2-Al_3	3.26770(6)
Sr_2-Al_3	3.26770(6)
Sr_2-Al_6	3.42209(9)

Reference

1. W. Geng, X. Zhou, J. Ding, G. Li and Y. Wang, *Journal of Materials Chemistry C*, 2017, **5**, 11605-11613.
2. H. Chen and Y. Wang, *Journal of the American Ceramic Society*, 2021, **105**, 1095-1105.
3. L. G. Vanuitert, *Journal of Luminescence*, 1984, **29**, 1-9.
4. X. Ma, P. Feng, Y. Wang, S. Ding, S. Tian and Y. Wang, *Journal of Materials Chemistry C*, 2022, **10**, 1105-1117.
5. S. Liang, M. Shang, H. Lian, K. Li, Y. Zhang and J. Lin, *Journal of Materials Chemistry C*, 2016, **4**, 6409-6416.
6. Z. Kang, S. Wang, T. Seto and Y. Wang, *Advanced Optical Materials*, 2021, **9**.